PROCEEDINGS OF SCIENCE

Can γ-rays be detected from accretion-driven magnetic systems?

Spencer T. Madzime[a,*] **and Pieter J. Meintjes**[a]

[a] *University of the Free State,*
205 Nelson Mandela Dr, Park West, Bloemfontein, South Africa

E-mail: tsmadzime@gmail.com, MeintjPJ@ufs.ac.za

Historical reports of pulsed TeV emission from AM Herculis, although later ruled out, led to a search for GeV signatures in magnetically controlled accreting white dwarf binaries using time-resolved analysis techniques with Fermi-LAT data. We present a Fermi-LAT analysis of accretion-driven magnetic systems (Polars: CV Hyi, AN UMa, AR UMa, and IPs: V515 And, and XY Ari), applying time-resolved (binned likelihood analysis together with TS-gating technique), and temporal analysis to isolate transient gamma-ray signals. Although no persistent emission was detected at the $> 5\ \sigma$ level in time-integrated searches, of the above mentioned systems exhibit significant gamma-ray excesses that are spatially coincident with the celestial location of each accretion-driven magnetic system when TS-gated data was considered. The detection of transient, low-level gamma-ray emitters was made possible by the 15-year cadence and sensitivity of the Fermi-LAT. Notably, CV Hyi shows a TS of 203.69 with a weighted significance of $\sigma_w = 5.3\ \sigma$, and an orbital modulation at 1.269 ± 0.004 hrs, with a detection significance of $5.3\ \sigma$. AN UMa (TS = 237.35; $\sigma_w = 5.9\ \sigma$) displays a significant $5.2\ \sigma$ orbital modulation at 1.907 ± 0.037 hrs, while AR UMa (TS = 149.95; $\sigma_w = 4.6\ \sigma$) reveals a $6.4\ \sigma$ periodic signal at 1.949 ± 0.055 hrs distinct from its optical double-peaked profile. Intermediate Polars, V515 And (TS = 227.05; $\sigma_w = 5.7\ \sigma$) exhibits pulsed γ-ray emission at the white dwarf spin period (465.162 ± 1.364 s; $6.7\ \sigma$), and XY Ari (TS = 195.52; $\sigma_w = 5.3\ \sigma$) shows modulation at 206.229 ± 0.115 s ($5.3\ \sigma$). Future studies with more sensitive gamma-ray observatories such as CTA, AMEGO, or e-ASTROGAM, complemented by X-ray and optical monitoring, could provide additional observational data to constrain particle acceleration mechanisms responsible for the emission in these compact binaries.

High Energy Astrophysics in Southern Africa (HEASA2025)
16-20 September, 2025
University of Johannesburg, South Africa

*Speaker

 ISSN 1824-8039 . Published by SISSA Medialab.

PoS(HEASA2025)068

1. Introduction

Magnetically controlled accreting white dwarfs, including polars and intermediate polars (IPs), are important astrophysical objects for studying particle acceleration mechanisms under accretion-driven conditions. Their strong magnetic fields (1–230 MG [1]), rapid rotation, and dynamic plasma environments allow for a variety of high-energy acceleration processes. In polars, where the white dwarf spin is synchronously locked to the orbital motion, particle acceleration may occur through unipolar induction during episodes of mild asynchronism or through diffusive shock acceleration in magnetically confined accretion columns [2, 3]. In IPs, magnetic reconnection at the disk magnetosphere interface can sustain relativistic particle acceleration, which may lead to nonthermal radiation extending from the optical to the gamma-ray regime [4].

Historical reports of transient optical and TeV activity in systems such as AM Her and AE Aqr [5, 6] suggested that white dwarfs could act as low-luminosity analogues of pulsars. However, these detections were often transient and were not confirmed by later observations e.g., [7]. The launch of the Fermi Large Area Telescope (LAT) provided a powerful means to revisit these systems with much better temporal cadence and sensitivity in the 0.1 to 500 GeV energy range. Previous LAT-based searches have revealed possible evidence of gamma-ray emission from several magnetic cataclysmic variables (MCVs), including AE Aqr (e.g., [8, 9], AR Sco (e.g., [10, 11]), and additional candidates (e.g., LAMOST J024048.51+195226.9 and CTCV J2056−3014, EUVE J0317-85.5, [12, 13]). Most of these studies employed time-averaged likelihood analyses, which, although statistically robust for bright sources, may obscure transient emission. This motivates the use of a time-resolved (e.g., TS-gating, [12]) analysis approach that can isolate periodic or duty cycle limited gamma-ray components.

In this study we present a systematic Fermi LAT investigation of a representative sample of strongly magnetized white dwarfs, including both polars and intermediate polars. We apply a combination of time-integrated likelihood, TS-gating, and periodic analyses to search for persistent and transient gamma-ray signals that coincide with the positions of these systems.

2. Fermi LAT Data Reduction and Analysis

Fermi LAT data were reduced and analyzed using standard likelihood techniques complemented by a TS-gating procedure to enhance the detection of faint or episodic sources. Gamma-ray events in the 0.1–500 GeV range were selected within a 10° region of interest (ROI), with a zenith angle cut of $< 90°$. SOURCE-class events (evclass=128) with FRONT+BACK conversions (evtype=3) were analyzed using the P8R3_SOURCE_V2_v1 instrument response functions. Livetime cubes and exposure maps were generated, and a binned likelihood analysis [14] was performed using `gtlike`/`pyLikelihood`, and `fermipy`.

While standard likelihood analysis effectively recovers steady emission, faint or transient sources often remain below the LAT detection threshold due to the diffuse background or nearby bright sources. To mitigate this, we employed TS-gating, which enhances the visibility of episodic or transient emission that occasionally rises above the background ([12]), inspired by pulsar phase-gating techniques e.g., [15]. Instead of gating in rotational phase, TS-gating identifies short intervals in the light curve where the likelihood analysis yields TS > 0, isolating periods when the emission

is statistically distinguishable from the background. Typically, only a fraction of the light curve satisfies this criterion ($\alpha \sim 0.3$), and restricting analysis to these intervals enhances the visibility of faint emission in the binned likelihood, spectral, and spatial analyses. Candidate sources in the gated dataset were verified using the `find_sources` routine in `fermipy` [16], used to search for all point sources above a certain threshold. To correct for the bias introduced by selecting intervals with increased gamma ray activities, we adopt a duty-cycle weighted significance [12]:

$$\sigma_w \approx \alpha \sqrt{\sum_{0.1\,\mathrm{GeV}}^{500\,\mathrm{GeV}} \left[TS_{\mathrm{gated}}(E) - TS_{\mathrm{ungated}}(E)\right]}, \tag{1}$$

where $TS_{\mathrm{gated}}(E)$ and $TS_{\mathrm{ungated}}(E)$ are summed over energy bins. This provides a more conservative estimate of the true detection significance, accounting for selection bias. For the initial exploration using the binned likelihood analysis, we adopted a simple PowerLaw model to describe the source of interest. The PowerLaw was chosen because it represents the basic nonthermal spectral model and is commonly used as a starting point to explore the general spectral shape. It allows us to establish a baseline for the overall flux distribution and to determine the energy range where the emission remains statistically significant. In subsequent refinements, we also applied the LogParabola and PLSuperExpCutoff2 models to produce and fit the flux points, thereby investigating the structure of the spectral energy distribution (SED) and identifying the characteristic cutoff energy beyond which the emission falls below detection limits. Understanding this energy range is essential for optimizing the subsequent periodicity search, which was restricted to the most relevant energy bands to enhance sensitivity to potential periodic modulation.

However, in our results, we present only the binned likelihood results obtained with the source of interest modeled using the LogParabola model. For the spectral plots, we present the LogParabola fits, as this model upon inspection by eye provided better overall fits and narrower butterfly plots compared to the alternative pulsar model (PLSuperExpCutoff2), and the PowerLaw. In the SEDs plots, flux points with a detection significance below 2σ were treated as upper limits. Consequently, the energy at which the data transition into upper limits marks the approximate cutoff energy of the source emission.

Finally, to validate potential TS-gated detections, timing analyses were performed on the ungated data using a 0.6° ROI and energies of 0.1–20 GeV. Photon arrival times were barycentered, and periodicity searches were conducted with `gtpsearch` and the Tempo2 Fermi plug-in [17, 18]. This approach allowed verification that faint gamma-ray excesses identified with TS-gating are consistent with spin or orbital modulated emission from the target sources, rather than random fluctuations or unrelated background. The mean period and its uncertainty were derived from multiple periodograms computed over slightly varied energy ranges. Starting with the primary range of 0.1–20 GeV, the lower bound was incrementally varied from 0.1 GeV to 2 GeV in 0.1 GeV steps, while the upper bound remained fixed at 20 GeV. For each configuration, the frequency corresponding to the maximum Test Statistic (TS) was recorded. The mean and standard deviation of these frequencies, $\bar{f}$ and σ_f, were used to compute the mean period and its uncertainty through $\sigma_P = \sigma_f / \bar{f}^2$, where the mean period is the inverse of $\bar{f}$.

3. Results and Discussion

The Fermi LAT analysis of the TS-gated data of five magnetic cataclysmic variables (Polars: CV Hyi, AN UMa, AR UMa, and IPs: V515 And, and XY Ari) reveals statistically significant gamma-ray excesses in the 0.1–500 GeV range. Table 1 summarises the results of the binned likelihood analysis performed on the TS-gated data using a LogParabola spectral model for the sources of interest.

Table 1: Results of the binned likelihood analysis for selected accretion-driven magnetic systems (polars: black, and IPs: red), obtained with the source of interest modeled using a LogParabola spectrum. Columns are: test statistic (TS), number of predicted counts (Npred), integrated energy flux in the 0.1–500 GeV band (erg cm^{-2} s^{-1}), positional offset from the catalog position (deg), weighted detection significance σ_w, and best-fit celestial coordinates (RA, Dec) given in decimal degrees (J2000).

Source	TS	Npred	Flux (erg cm^{-2} s^{-1})	Offset	σ_w	RA	Dec
Polars							
CV Hyi	203.69	854.96	$1.13 \pm 0.239 \times 10^{-8}$	0.066	5.3	23.3324	−65.923
AN UMa	237.35	1352.11	$1.54 \pm 0.296 \times 10^{-8}$	0.098	5.9	166.2249	45.105
AR UMa	149.95	1021.34	$1.12 \pm 0.256 \times 10^{-8}$	0.155	4.6	168.7718	43.071
IPs							
V515 And	227.05	1527.31	$1.70 \pm 0.544 \times 10^{-8}$	0.049	5.7	13.8047	46.261
XY Ari	195.52	1263.71	$1.48 \pm 0.288 \times 10^{-8}$	0.026	5.3	44.0565	19.458

For each source, a standard set of diagnostic plots illustrates the spectral, and timing results from this study. Figure 1 (Polars) and Figure 2 (IPs) present the Fermi-LAT spectra modeled with a LogParabola (first column), while the corresponding TS versus energy distributions for gated (black) and ungated (red) data are shown in the adjacent (second) column. The weighted significance, calculated from Equation 1, is also shown in the TS vs Energy plots and it quantifies the detection confidence.

Table 2: Results of the timing analysis for the selected accretion-driven magnetic systems, polars (black), and IPs (red). Listed are the mean detected periods, corresponding detection significances (σ), and reference epochs T_0 given in both modified Julian date (MJD; for the Fermi plugin and Tempo2) and heliocentric or barycentric Julian date (HJD or BJD), together with the corresponding literature references.

Source	Period	σ	$T_{0,MJD}$	T_0
Polars				
CV Hyi	1.269 ± 0.004 hr	5.3	T_{MJD} = 50047.163491	T_{HJD} = 2450047.6628 [19]
AN UMa	1.907 ± 0.037 hr	5.2	T_{MJD} = 43190.492644	T_{BJD} = 2443190.9926 [20–22]
AR UMa	1.949 ± 0.055 hr	6.4	T_{MJD} = 50469.931660	T_{HJD} = 2450470.4309 [22, 23]
IPs				
V515 And	465.162 ± 1.364 s	6.7	T_{MJD} = 54742.646425	T_{BJD} = 2454743.146425 [24]
XY Ari	206.229 ± 0.115 s	5.3	T_{MJD} = 50276.903820	T_{BJD} = 2450277.40382 [25]

Table 2 lists the average detected periods from the Rayleigh folding test, their detection significances, and the reference epochs T_0 used in the folding analyses. The timing plots in Figure 1

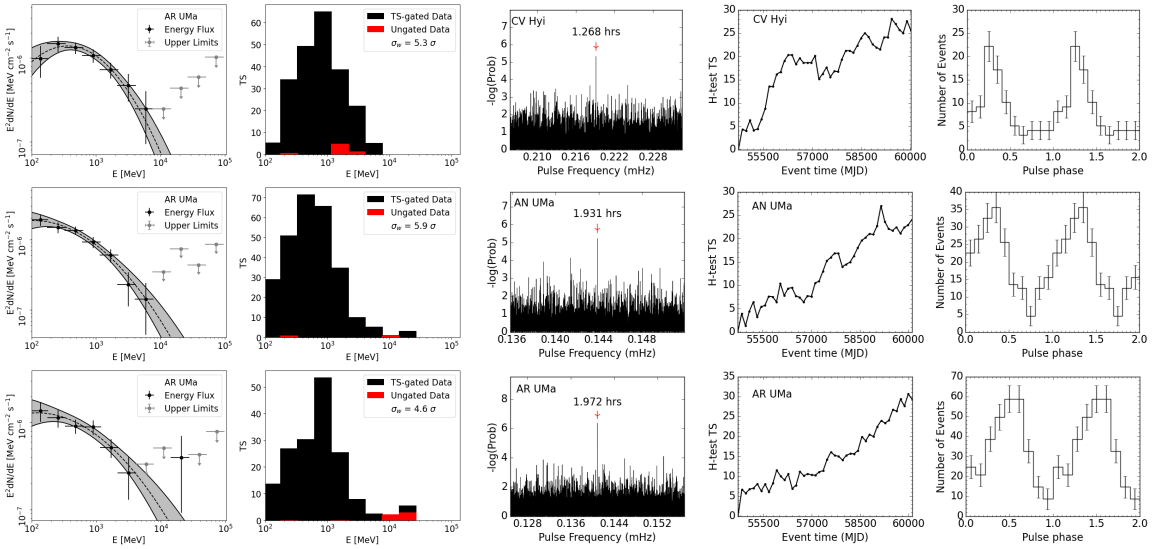

Figure 1: Polars: For each source, the first column shows the Fermi-LAT spectra modeled with a Log-Parabola, and the second column shows the corresponding TS versus energy distributions for gated (black) and ungated (red) data. The third column presents the Rayleigh power spectra indicating peaks at the orbital periods, the fourth column shows the H-test curves illustrating the accumulation of pulsed events, and the fifth column displays binned phase-folded light curves showing the photon distribution over orbital cycles. The rows corresponds to: First row, CV Hyi; second row, AN UMa; third row, and AR UMa.

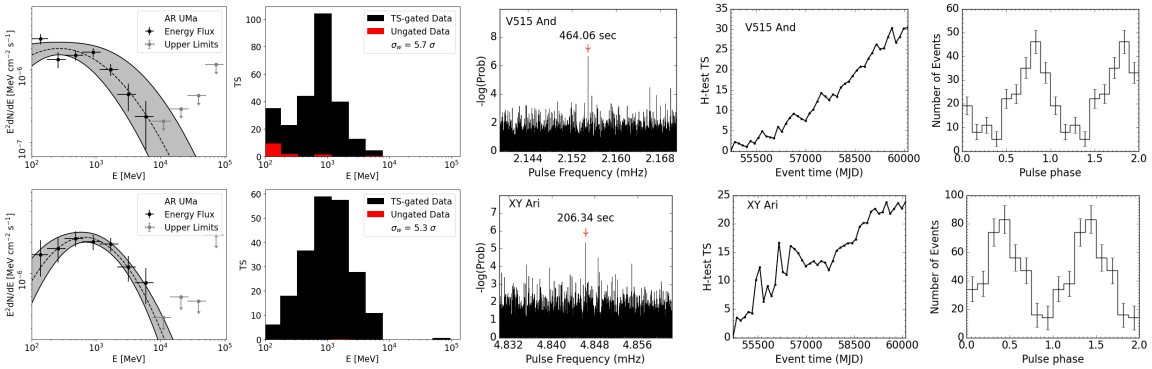

Figure 2: IPs: The first column displays the Fermi-LAT spectra fitted with a LogParabola, and the second column displays the accompanying TS versus energy distributions for gated (black) and ungated (red) data. Third column shows the Rayleigh power spectra illustrating peaks at the spin periods, the fourth column shows the H-test curves demonstrating the accumulation of pulsed events, and the fifth column displays binned phase-folded light curves pulsed modulation over the spin cycles. The rows corresponds to: First row, V515 And, and second row, XY Ari.

(Polars) and Figure 2 (IPs) display the Rayleigh power spectra (third column), indicating peaks at the spin or orbital periods; the H-test curves (fourth column), showing the accumulation of pulsed events; and the phase-folded light curves (fifth column), illustrating the photon distribution over the spin or orbital cycles. Phase-folded light curves were constructed using published ephemerides: CV Hyi [19], AN UMa [20], AR UMa [23], V515 And [24], and XY Ari [25]. All sources show coherent modulation consistent with their known optical periodicities. In AR UMa, the GeV light curve displays a single maximum, in contrast to the double-peaked optical/IR structure [23].

4. Conclusion

The detection of statistically significant gamma-ray excesses from both polar and intermediate polar systems in our sample using TS-gating, made possible by the 15-year baseline of the LAT, provides compelling evidence that accretion-driven magnetic white dwarfs can act as recurrent, though low-luminosity, high-energy sources. The spectral and timing characteristics, nonthermal emission peaking below ∼10 GeV, and modulation at the white dwarf spin/orbital period, are consistent with magnetospheric acceleration processes. The unipolar inductor model was proposed to explain nonthermal emission in polars, including radio emission and the potential GeV gamma rays reported in this study, under conditions of mild asynchronism, where significant electric potentials can develop across the stellar surface, driving relativistic particle acceleration [2]. In intermediate polars, magnetic reconnection at the disk–magnetosphere boundary was also proposed to explain particle acceleration and the subsequent production of X-ray tails and GeV gamma rays through hadronic channels [4]. A definitive verdict on the dominant acceleration mechanism will require systematic, multiwavelength campaigns that combine contemporaneous optical, X-ray, and gamma-ray monitoring with detailed magnetohydrodynamic modeling to disentangle the competing processes. At present, the results strongly support a hybrid framework in which unipolar induction and reconnection driven acceleration together shape the high energy behavior of magnetic cataclysmic variables.

References

[1] G. D. Schmidt, P. Szkody, P. S. Smith, A. Silber, G. Tovmassian, D. Hoard et al., *ApJ* **473** (1996) 483.

[2] S. T. Madzime and P. J. Meintjes, *PoS* **HEASA2023** (2024) 021.

[3] C. Kaul, R. Kaul and C. Bhat, *A&A* **272** (1993) 501.

[4] W. Bednarek and J. Pabich, *MNRAS* **411** (2011) 1701.

[5] C. Bhat, R. Kaul, H. Rawat, V. Senecha, R. Rannot, M. Sapru et al., *ApJ* **369** (1991) 475.

[6] P. Meintjes, O. De Jager, B. Raubenheimer, H. Nel, A. North, D. Buckley et al., *ApJ* **434** (1994) 292.

[7] J. Aleksić, S. Ansoldi, L. A. Antonelli, P. Antoranz, A. Babic, P. Bangale et al., *A&A* **568** (2014) A109.

[8] S. T. Madzime, P. Meintjes, H. van Heerden, K. K. Singh, D. Buckley, P. Woudt et al., *PoS* **HEASA2021** (2021) 046.

[9] J. Li, D. F. Torres, N. Rea, E. de Ona Wilhelmi, A. Papitto, X. Hou et al., *ApJ* **832** (2016) 35.

[10] Q. Kaplan, P. J. Meintjes, K. K. Singh, H. J. van Heerden, F. A. Ramamonjisoa and I. P. van der Westhuizen, *PoS* **ICRC2019** (2021) 602 [1908.00283].

[11] P. J. Meintjes, S. T. Madzime, Q. Kaplan and H. J. van Heerden, *Galaxies* **11** (2023) 14.

[12] S. T. Madzime and P. Meintjes, *PoS* **HEASA2022** (2023) 055.

[13] L. Minnie, P. J. Meintjes and J. Maritz, *PoS* **HEASA2023** (2024) 011.

[14] J. R. Mattox, D. Bertsch, J. Chiang, B. Dingus, S. Digel, J. Esposito et al., *ApJ* **461** (1996) 396.

[15] M. Arakawa, M. Hayashida, D. Khangulyan and Y. Uchiyama, *ApJ* **897** (2020) 33.

[16] M. Wood, R. Caputo, E. Charles, M. Di Mauro, J. Magill and J. Perkins, *arXiv preprint arXiv:1707.09551* (2017) .

[17] G. Hobbs, R. Edwards and R. Manchester, *MNRAS* **369** (2006) 655.

[18] P. S. Ray, M. Kerr, D. Parent, A. Abdo, L. Guillemot, S. Ransom et al., *ApJS* **194** (2011) 17.

[19] V. Burwitz, K. Reinsch, K. Beuermann and H.-C. Thomas, *A&A* **327** (1997) 183.

[20] J. Bonnet-Bidaud, M. Mouchet, T. Somova and N. Somov, *A&A* **306** (1996) 199.

[21] S. Ok, M. Yardımcı, B. Kalomeni and A. Schwope, *MNRAS* **541** (2025) 1913.

[22] B. Kalomeni, *MNRAS* **422** (2012) 1601.

[23] S. B. Howell, D. M. Gelino and T. E. Harrison, *AJ* **121** (2001) 482.

[24] V. Kozhevnikov, *MNRAS* **422** (2012) 1518.

[25] C. Hellier, K. Mukai and A. Beardmore, *MNRAS* **292** (1997) 397.